ISSN 1674-1056
http://cpb.iphy.ac.cn
http://iopscience.iop.org/cpb
中国物理 B
Chinese Physics
中国物理 Chinese Physics B

Photoinduced phase transitions in two-dimensional charge-density-wave 1T-TaS_2

Wen Wen(文雯), Chunhe Dang(党春鹤), Liming Xie(谢黎明)

Citation: Chin. Phys. B . 2019, 28(5): 058504. **doi:** 10.1088/1674-1056/28/5/058504
Journal homepage: http://cpb.iphy.ac.cn; http://iopscience.iop.org/cpb

What follows is a list of articles you may be interested in

Ultraviolet photodetectors based on wide bandgap oxide semiconductor films

Changqi Zhou(周长祺), Qiu Ai(艾秋), Xing Chen(陈星), Xiaohong Gao(高晓红), Kewei Liu(刘可为), Dezhen Shen(申德振)
Chin. Phys. B . 2019, 28(4): 048503. **doi:** 10.1088/1674-1056/28/4/048503

Effect of temperature on photoresponse properties of solar-blind Schottky barrier diode photodetector based on single crystal Ga_2O_3

Chao Yang(杨超), Hongwei Liang(梁红伟), Zhenzhong Zhang(张振中), Xiaochuan Xia(夏晓川), Heqiu Zhang(张贺秋), Rensheng Shen(申人升), Yingmin Luo(骆英民), Guotong Du(杜国同)
Chin. Phys. B . 2019, 28(4): 048502. **doi:** 10.1088/1674-1056/28/4/048502

High quantum efficiency long-/long-wave dual-color type-Ⅱ InAs/GaSb infrared detector

Zhi Jiang(蒋志), Yao-Yao Sun(孙姚耀), Chun-Yan Guo(郭春妍), Yue-Xi Lv(吕粤希), Hong-Yue Hao(郝宏玥), Dong-Wei Jiang(蒋洞微), Guo-Wei Wang(王国伟), Ying-Qiang Xu(徐应强), Zhi-Chuan Niu(牛智川)
Chin. Phys. B . 2019, 28(3): 038504. **doi:** 10.1088/1674-1056/28/3/038504

Realizing photomultiplication-type organic photodetectors based on C_{60}-doped bulk heterojunction structure at low bias

Wei Gong(龚伟), Tao An(安涛), Xinying Liu(刘欣颖), Gang Lu(卢刚)
Chin. Phys. B . 2019, 28(3): 038501. **doi:** 10.1088/1674-1056/28/3/038501

Phase transition and charge transport through a triple dot device beyond the Kondo regime

Yong-Chen Xiong(熊永臣), Zhan-Wu Zhu(朱占武), Ze-Dong He(贺泽东)
Chin. Phys. B . 2018, 27(10): 108503. **doi:** 10.1088/1674-1056/27/10/108503

TOPICAL REVIEW — Photodetector: Materials, physics, and applications

Photoinduced phase transitions in two-dimensional charge-density-wave 1T-TaS_2*

Wen Wen(文雯)[1,2], Chunhe Dang(党春鹤)[1,2], and Liming Xie(谢黎明)[1,2,†]

[1] CAS Key Laboratory of Standardization and Measurement for Nanotechnology, CAS Center for Excellence in Nanoscience, National Center for Nanoscience and Technology, Beijing 100190, China

[2] University of Chinese Academy of Sciences, Beijing 100049, China

(Received 23 February 2019; revised manuscript received 18 March 2019; published online 8 April 2019)

Charge-density-wave (CDW) materials with strongly correlated electrons have broadband light absorption and ultrafast response to light irradiation, and hence hold great potential in photodetection. 1T-TaS_2 is a typical CDW material with various thermodynamically CDW ground states at different temperatures and fertile out-of-equilibrium intermediate/hidden states. In particular, the light pulses can trigger melting of CDW ordering and also forms hidden states, which exhibits strikingly different electrical conductivity compared to the ground phase. Here, we review the recent research on phase transitions in 1T-TaS_2 and their potential applications in photodetection. We also discuss the ultrafast melting of CDW ordering by ultrafast laser irradiation and the out-of-equilibrium intermediate/hidden states by optical/electrical pulse. For photodetection, demonstrations of photoconductors and bolometers are introduced. Finally, we discuss some of the challenges that remain.

Keywords: charge density wave, phase transition, 1T-TaS_2, photodetection

PACS: 85.60.Gz, 95.55.Rg, 71.45.Lr **DOI:** 10.1088/1674-1056/28/5/058504

1. Introduction to structure and charge-density waves in 1T-TaS_2

Low-dimensional strongly correlated electron systems arise from the couplings between charge, spin, and lattice. They exhibit rich phase transitions, such as superconductivity, ferromagnetism, and charge-density wave (CDW) ordering.[1–4] CDW states comprise a periodic charge-density modulation and a periodic lattice distortion, which originate from the electron–phonon interactions and/or Fermi surface nesting.[5–9] Due to the collective mode of charge density, a finite electronic bandgap opens with the forming of the CDW phase.[10–12]

The theory of the electron–phonon interaction of the CDW system was first suggested by Peierls in 1955.[6] For a one-dimensional (1D) metal chain at temperature $T = 0$ K without considering the electron–electron or electron–phonon interactions, the ground state is schematically presented in Fig. 1(a). The atomic chain possesses a lattice constant of a and the electronic states are filled up to the Fermi surface E_F. After taking electron–phonon interaction into consideration, the lattice distortion with a period of λ is more energetically favorable. The period λ is related to the Fermi wave vector k_F by $\lambda = \pi/k_F$. The lattice distortion opens a finite energy gap 2Δ at the Fermi level (Fig. 1(b)), thus turning the metallic phase into insulating CDW phase. Compared to the metallic phase with constant charge density of ρ_0, CDW states exhibit a periodic collective mode with modulated charge density, which can be expressed as[6]

$$\rho(\boldsymbol{r}) = \rho_0 + \rho_1 \cos(2\boldsymbol{k}_F \cdot \boldsymbol{r} + \varphi), \quad (1)$$

where ρ_1 and φ are the amplitude and phase of periodically modulated electron density, respectively, and $\boldsymbol{r}$ is the displacement.

1T-TaS_2, with a plane of Ta atoms sandwiched between two layers of S atoms in an octahedral lattice, exhibits temperature-dependent CDW orderings. At a temperature below 550 K, the incommensurate (IC) CDW phase forms with slightly distorted lattices. As the temperature is lower than 350 K, nearly commensurate (NC) CDW forms with insulating commensurate domains and conductive domain walls. Further lowering the temperature down to 180 K, insulating commensurate CDW (CCDW) phase occurs (Fig. 2(a)). In the CCDW phase, the lattice distortion is characterized by a $\sqrt{13} \times \sqrt{13}$ superlattice of David-stars comprised of 12 Ta atoms around a 13th Ta atom (Fig. 2(b)).

The resistance of 1T-TaS_2 changes in the different CDW states. For bulk crystal, two abrupt changes of resistance can be observed at temperatures of 180–220 K and 350–360 K, corresponding to CCDW–NCCDW and NCCDW–

*Project supported by the National Natural Science Foundation of China (Grant Nos. 21673058 and 21822502), the Key Research Program of Frontier Sciences of Chinese Academy of Sciences (Grant No. QYZDB-SSW-SYS031), and the Strategic Priority Research Program of Chinese Academy of Sciences (Grant No. XDB30000000).

†Corresponding author. E-mail: xielm@nanoctr.cn

© 2019 Chinese Physical Society and IOP Publishing Ltd

ICCDW phase transitions, respectively (Fig. 2(c)).[13] As the thickness of 1T-TaS_2 decreases, the NC–C phase transition disappears (Fig. 2(d)) as the thickness is less than 9 nm and 3 nm, respectively. The thickness-dependent phase transition behavior was explained as slow kinetics of phase transition.[14] It was further found that the NC-to-C phase transition process disappeared at high cooling rate.[14] Zhang and his colleagues attributed the thickness dependence to the periodicity for sustaining long-range order, dielectric environment, and surface impurities.[13]

The fertile phase transitions in 1T-TaS_2 have been investigated by versatile tools. For instance, the distribution of electronic density in real space, the configuration and electronic structure of domain walls, and the manipulation of CDW phases have been extensively studied by scanning tunneling microscopy.[15–19] The ultrafast photoemission spectroscopy has been introduced to monitor the dynamics of electronic structure in the phase transition process.[20–24] The ultrafast diffraction technique has been developed to reveal the lattice dynamics of CDW phase transition process.[25–27]

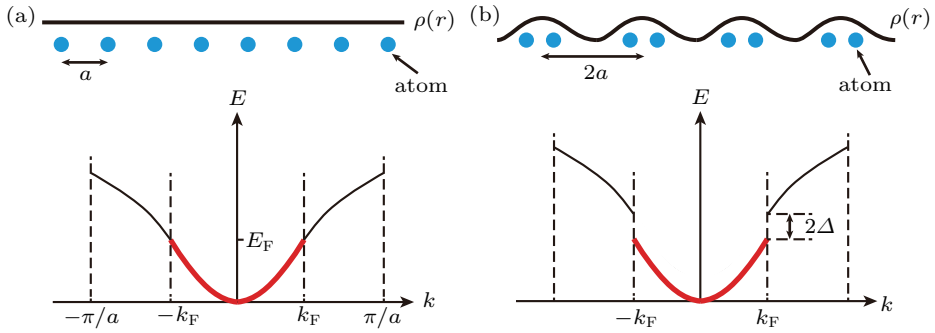


Fig. 1. Schematic illustration of one-dimensional periodic metallic lattice and Peierls distorted insulating lattice. (a) Without electron–phonon interaction, the lattice with a period of a exhibits a constant charge density and filled electron states up to Fermi level. (b) Considering the electron–phonon interaction, the Peierls distortion results in the periodically modulated charge density and an energy gap at the Fermi level. Reproduced from Ref. [6] with permission. Copyright 1988, American Physical Society.

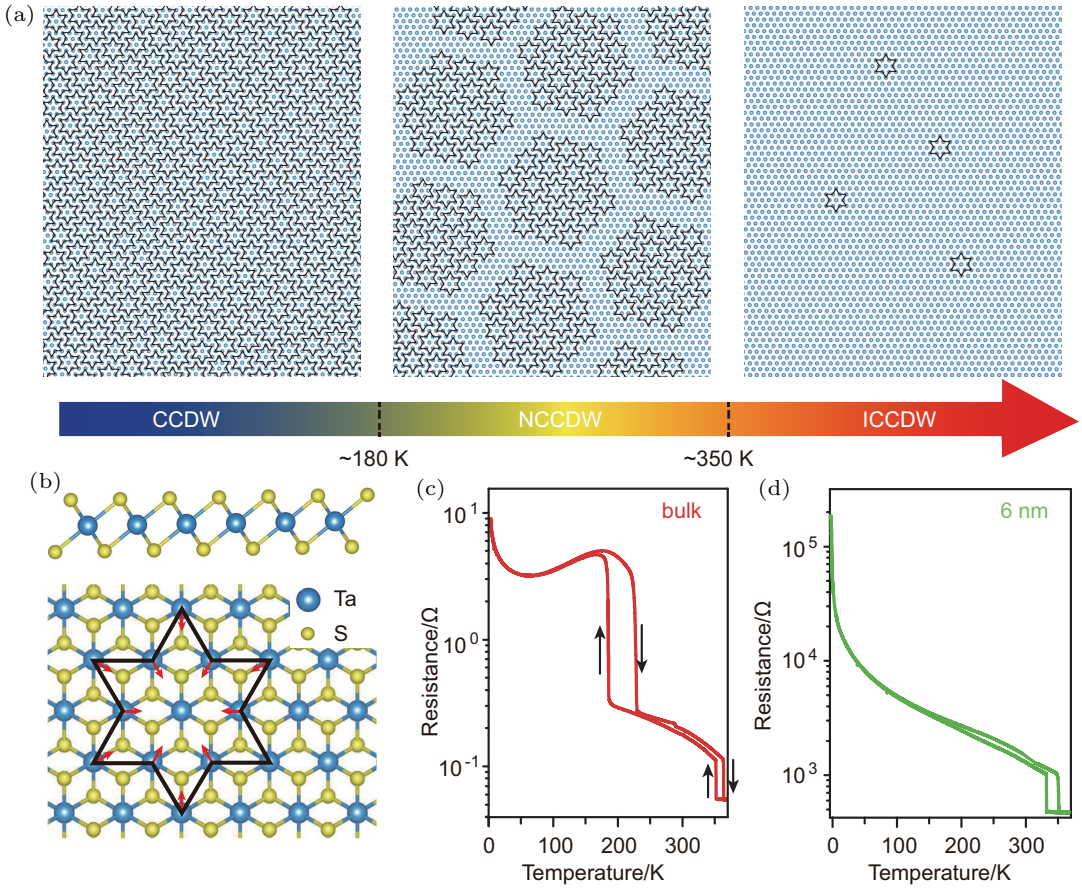


Fig. 2. CDW phase in 1T-TaS_2 at different temperatures. (a) The CCDW, NCCDW, and ICCDW phases at different temperatures. (b) Crystal structure of 1T-TaS_2 with David-star clusters consisting of 13 Ta atoms. (c) Temperature-dependent resistance of bulk 1T-TaS_2. (d) Temperature-dependent resistance of 1T-TaS_2 with thickness of 6 nm. As the thickness of 1T-TaS_2 decreases, the phase transition from NC to IC phase is unresolvable owing to the slow kinetics. (c) and (d) were reproduced from Ref. [13]. Copyright 2015, Springer Nature.

Additionally, Raman spectroscopy is sensitive to the collective lattice vibration, which has been demonstrated as an effective approach for measuring the CDW phase transition.[28–32] Compared to the undistorted metallic lattice, the commensurate domains consisting of $\sqrt{13} \times \sqrt{13}$ superlattice exhibit fold-back acoustic and optical modes with Raman frequency of 50–100 cm^{-1} and 230–400 cm^{-1}, respectively.[28] With the transition from CCDW–NCCDW phase, an abrupt red-shift of Raman peaks was observed.[30] In striking contrast to the electrical measurements, the Raman spectroscopy demonstrated that fold-back acoustic and optical modes are preserved in monolayer 1T-TaS_2. This result possibly suggests that CDW phase order can be stable at monolayer 1T-TaS_2.

Further electrical measurements have been conducted to investigate the correlation between the CDW states and electron transport properties. The significant change of electrical conductivity during the phase-transition process promises the characterization of dynamics of CDW states through electrical signals. For example, the low-frequency noise of electrical devices can be employed to understand the sliding of CDW domains.[33] Electrical oscillators, consisting of a 1T-TaS_2 device in serial with a load resistor, can be harnessed to study the dynamics of multistate phase transitions.[34,35]

Owing to the striking differences in electrical conductivity for various CDW states, the manipulation of CDW phases can be exploited to develop multifunctional devices. For example, Iwasa and his colleagues discovered a memristive NC-to-C phase switching behavior, arising from an extremely slow phase transition process with reduced thickness of 1T-TaS_2.[14,36] This work provided a proof-of-principle demonstration of nonvolatile memory devices based on the sluggish CDW phase transition of nano-thick 1T-TaS_2. The NC-to-IC phase transition is more attractive for the practical device implementations because it occurs at room temperature and can be triggered by optical pulses or electrical current. By collecting a 1T-TaS_2 in serial with a load resistor, electrical oscillation can be achieved by revisable switching between NC and IC phases.[34] Compared to the conventional ring oscillators, the CDW oscillators based on phase transition possess much simplified electrical circuits. Therefore, multiple CDW phase transition of 1T-TaS_2, together with its electrical/optical manipulability and low dimensionality, permits 1T-TaS_2 as a platform for fabrication of multifunctional phase-transition devices.

In addition to thermodynamic ground states at different temperatures, light pulses can drive the CDW phase transition and create fertile out-of-equilibrium intermediate states. For the phase transition triggered by light pulses, two effects will contribute to the collapse of highly ordered commensurate domains. First, the photo-injected electrons can fill the Mott–Hubbard bands, yielding mobile carriers to screen the Coulomb interaction between Ta atoms. With the collapse of Ta clusters and strongly correlated electronic states, highly conductive metal states can nucleate and grow. Second, high-fluence photon injection can give rise to Joule heating effect, which will increase the local temperature of the sample. Because the local temperature is higher than the phase-transition temperature, melting of CDW domain occurs. Therefore, special light–matter interactions can be observed in the CDW phases with strongly correlated electron system.

In this review, we have summarized the recent progress on the photoinduced CDW phase transitions in 1T-TaS_2, as well as the potential applications. First, the dynamics of optical pulse induced CDW phase transition in 1T-TaS_2 is introduced. Second, the out-of-equilibrium intermediate/hidden states, which can only be accessible by applying external stimuli, such as ultrafast laser pulses and electric field, are introduced. Third, potential applications of 1T-TaS_2 as photodetectors are introduced. Finally, we have prospected challenges and potential applications based on photoinduced CDW phase transitions.

2. Ultrafast optical pulse induced CDW phase transitions in 1T-TaS_2

Phase-transition dynamics in 1T-TaS_2 have been extensively studied by ultrafast optical stimulation. Femtosecond electron diffraction was used as a powerful tool to investigate the dynamics of crystal lattice during optical pulse induced phase transition. In the experiments, femtosecond laser pulses were employed to initiate the phase transition of 1T-TaS_2 from a highly ordered phase to a lowly ordered phase and an ultrafast electron beam was used to probe the lattice dynamics.[25,27] The dynamic melting, switching, and recovery processes have been extensively studied with this technique. In addition to electron diffraction, time-resolved x-ray photoelectron spectroscopy is another effective approach for investigating the evolution of CDW ordering under optical excitation. These ultrafast measurements employed different probes, such as x-ray and electron beams, to collect signals characterizing the structural dynamics, while using femtosecond light as a pump source to trigger the CDW phase transition.

At room temperature, the ground state of 1T-TaS_2 is the NCCDW phase, which possesses commensurate CDW domains reflected by $\sim 12^{\circ}$-rotated diffraction peaks in electron diffraction patterns (Fig. 3(a)). Under the light excitation exceeding a threshold, the melting of CDW domains occurs,

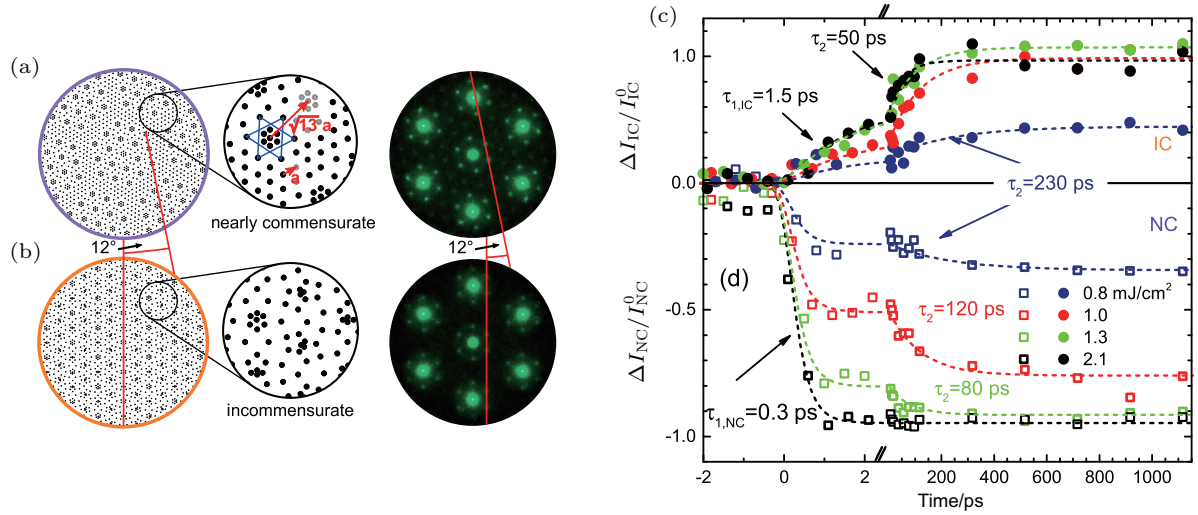


Fig. 3. The ultrafast optical pulse induced NC-to-IC phase transition of 1T-TaS_2 monitored by ultrafast electron diffraction. Real and reciprocal space representation of (a) NCCDW phase, and (b) ICCDW phase. Compared to the ICCDW with slight lattice distortion, the NCCDW phase consists of commensurate supercells, which exhibits $\sim 12°$-rotated high-order diffraction peaks. (c) The evolution of NC and IC intensities under different excitation densities. This figure was reproduced from Ref. [25] with permission. Copyright 2016, American Physical Society.

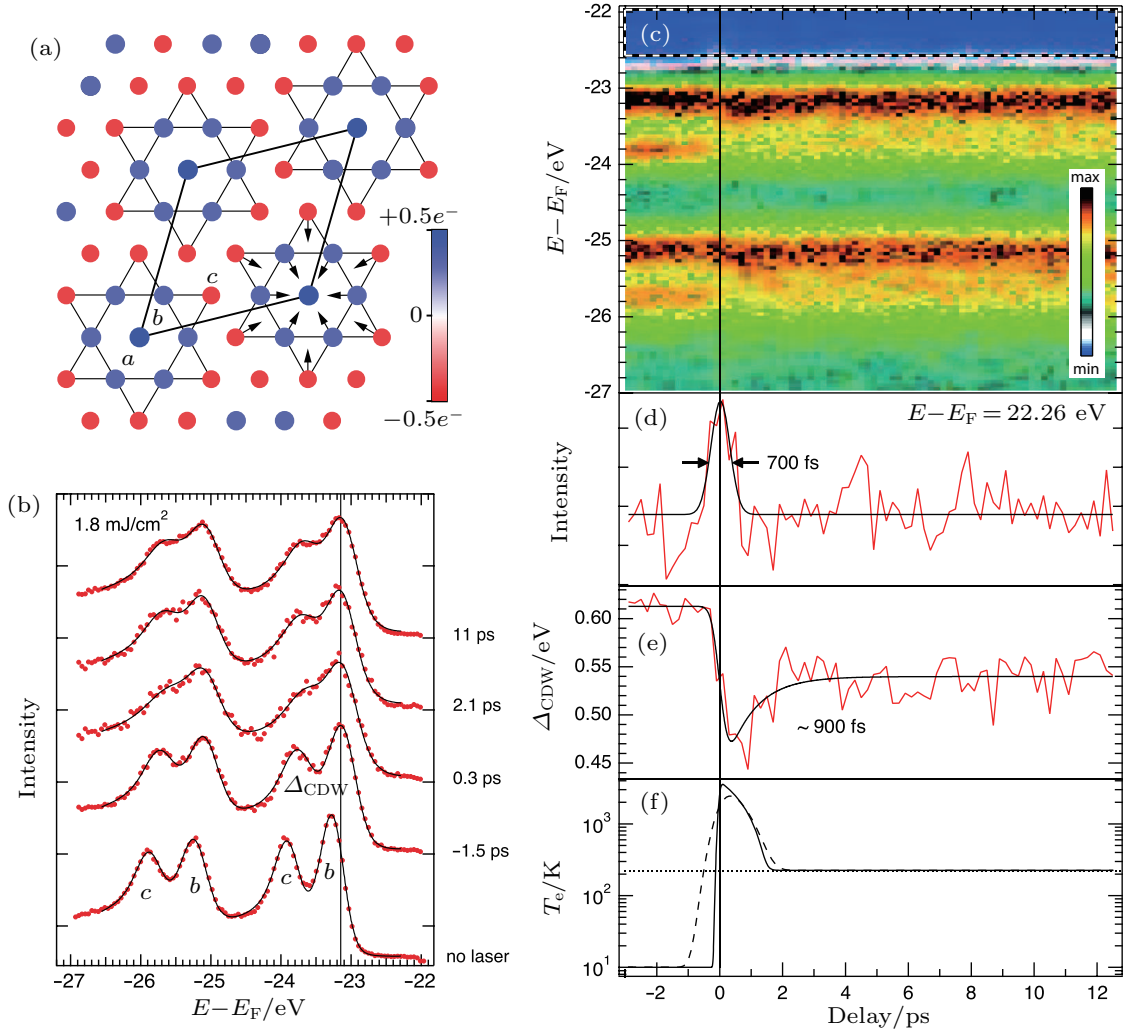


Fig. 4. The ultrafast optical pulse induced CDW phase transition monitored by time-resolved x-ray photoemission spectroscopy (TR-XPS). (a) Scheme of CCDW 1T-TaS_2 consisting of David-star clusters with inequivalent *a*, *b*, and *c* Ta atoms. (b) Ta 4f XPS spectra at different delay times. The color represents the electron density, which increases towards the center Ta atom. The Ta 4f photoemission is split into two peaks, corresponding to sites *b* and *c*, separated by 2Δ (i.e., Δ_{CDW}). (c) Two-dimensional false color map of Ta 4f photoemission spectra at different delays. (d) Time-resolved photoemission intensity at $E - E_F = -22.26$ eV. (e) Dependence of $2\Delta_{CDW}$ on the delay time. (f) Delay-time-dependent electron temperature T_e. This figure was reproduced from Ref. [23] with permission. Copyright 2010, American Physical Society.

reflected by the suppressed diffraction of NC superlattice and enhanced diffraction of IC phase (Fig. 3(b)). By extracting the time evolution of NC and IC intensities, a two-stage phase transition process has been discovered. In the first stage, the drop of NC diffraction intensity and the rise of IC intensity occur within 0.3 ps and 1.5 ps, respectively, which is independent of the pump fluence. In the second stage, the drop/rise of NC/IC intensity keeps ranging from 50 ps to 230 ps depending on the excitation power. The two-step melting of NC and buildup of IC phase are attributed to the nucleation of new phase followed by the domain growth.

The pump-fluence-independent nucleation rate indicates the absence of a nucleation barrier at the first stage. The dynamics of phase transition was proposed by Haupt *et al.* by combining the experimental results and theoretical calculations. They found that the changes in ionic potential, arising from the femtosecond laser excitation, give rise to the coherent atomic motion in commensurate domains towards the undistorted metallic domain walls. At the time scale of ~ 1 ps, the energy dissipation to lattice results in the rise of lattice temperature beyond the critical temperature of NC-to-IC phase transition. Further growth of IC phase requires much atomic displacement with the transformation of the previously commensurate domains. Overall, complete transformation of NC to IC phase occurs within the time of ~ 50 ps and can be explained by the nucleation and growth mechanism.

In addition to the ultrafast electron diffraction, time-resolved x-ray photoemission spectroscopy (TR-XPS) is another effective approach for investigating the dynamics of CDW phase transition.[23] This method employs three inequivalent Ta sites (labeled as *a*, *b*, and *c* in Fig. 4(a)) in CCDW 1T-TaS_2. In the 13-atom David-star clusters, about 0.4 electrons are transferred from outer 6 Ta atoms to inner ones. The charge transfer in CCDW phase is reflected by the split Ta 4f peaks in XPS spectra (Fig. 4(b)), which can be assigned to *b* and *c* sites (peak related to *a* site is weak to be resolved). The *b*–*c* splitting 2Δ can be extracted to characterize the CCDW phase order. Beye *et al.* performed the TR-XPS with a free-electron x-ray laser at ~ 156 eV as probe in combination with a synchronized optical pump laser at 1.55 eV as pump. Figure 4(b) shows the evolution of XPS spectra at different pump–probe delays. The Ta 4f splitting experiences an obvious reduction within a picosecond followed by partial recovery and formation of a quasi-equilibrium state with a lifetime longer than 10 ps. Figure 4(c) shows the false-color TR-XPS spectra. The 2Δ decreases from the original value of 0.62 eV to 0.47 eV, and then recovers to a quasi-equilibrium value of 0.54 eV with a time constant of ~ 900 fs. The lattice temperature was calculated and the quasi-equilibrium temperature was 226 K. The ultrafast TR-XPS can be explained by two processes. The first process is the transient collapse of charge order by filling of the Mott–Hubbard band and collapse of the Mott phase, reflected by the transient heating of electrons. Then, cooling of electrons occurs through transferring energy of crystal lattice, yielding a quasi-equilibrium state.

3. Hidden CDW phases in 1T-TaS_2

A single ultrafast laser pulse can also trigger the formation of hidden states with well-organized CDW domains and undistorted metallic domain walls in 1T-TaS_2. Stojchevska *et al.* reported the generation of a metallic hidden states at 1.5 K by applying a 35-fs laser pulse.[37] At temperatures below 180 K, 1T-TaS_2 exhibits an insulating CCDW state. After applying a 35-fs laser pulse exceeding the power threshold, an abrupt drop of resistance was observed, suggesting a phase transition from CCDW to a hidden state (Fig. 5(a)).[38] A constant resistance has been observed up to temperature of 60 K. Upon 100 K, the resistance is close to that of the C state. The hidden states can be erased by a train of 10^4 50-ps pulses.

A mechanism of the hidden-state formation is proposed by combining the experimental results and theoretical considerations. In CCDW states, the electronic states are contributed by the Ta d bands. The 12 electrons contributed by the 12 Ta atoms form occupied states, while the 13th electron is localized at the center Ta atom. The empty upper Hubbard bands and filled lower ones are generated by the 13th electron and open an energy gap to sustain the insulating CCDW state (Fig. 5(b)). After an ultrafast laser pulse, the injected electrons and holes fill the upper and lower Hubbard bands after ultrafast intraband thermalization, thus inducing the melting of C clusters. The organization of insulating CCDW domains and domain walls after the partial breakdown of the David-star clusters promote the formation of a long-range ordered hidden state. Note that this model is consistent with experimental results and theoretical understandings. However, direct characterization of the C domain structure in this hidden state is required to provide deep understandings in its formation mechanism and physical properties.

The electric field can also be harnessed to trigger phase transitions in 1T-TaS_2.[39–42] Vaskivskyi *et al.* reported the buildup of the conductive hidden states by pulsed current injection.[39] The current pulse passed through the sample can turn the insulating CCDW phase to a metallic hidden state with a high switching speed (30 ps), which provided a proof-of-principle demonstration of CDW phase transition for non-volatile memory.

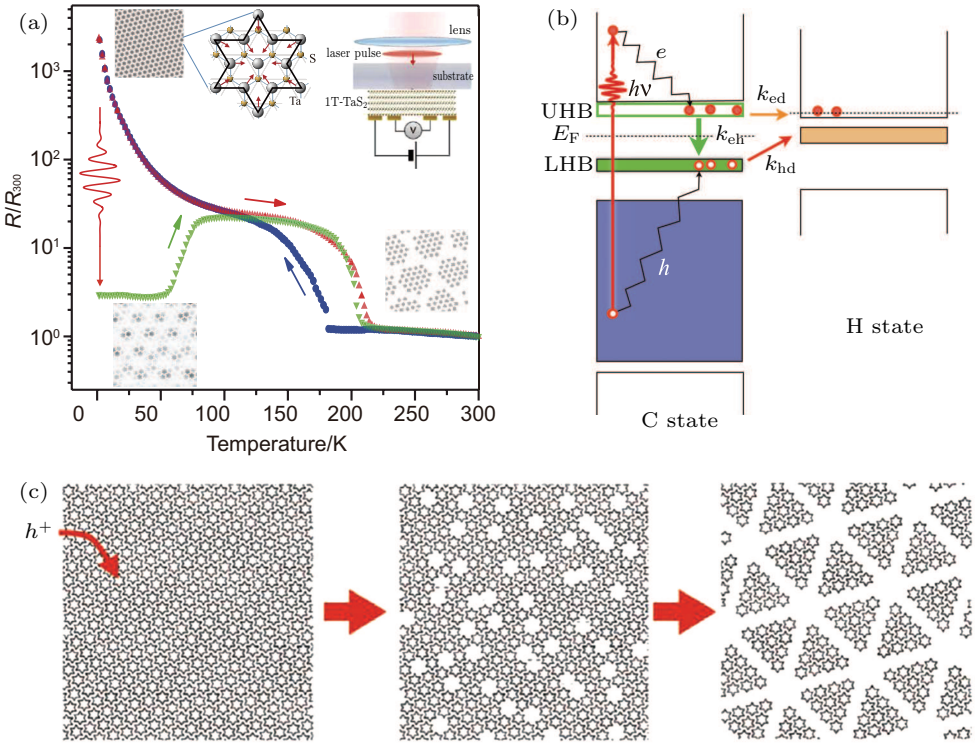


Fig. 5. The buildup of a hidden state by applying a 35-fs laser pulse. (a) An abrupt drop of electrical resistance can be observed after a single 35-fs laser pulse, which can be attributed to the formation of a hidden state. (b) Representation of energy diagram presents the buildup of the hidden states. (c) The phase diagram after a 35-fs laser pulse. (a) was reproduced from Ref. [38] with permission. (b) and (c) were reproduced from Ref. [37] with permission. Copyright 2014, AAAS.

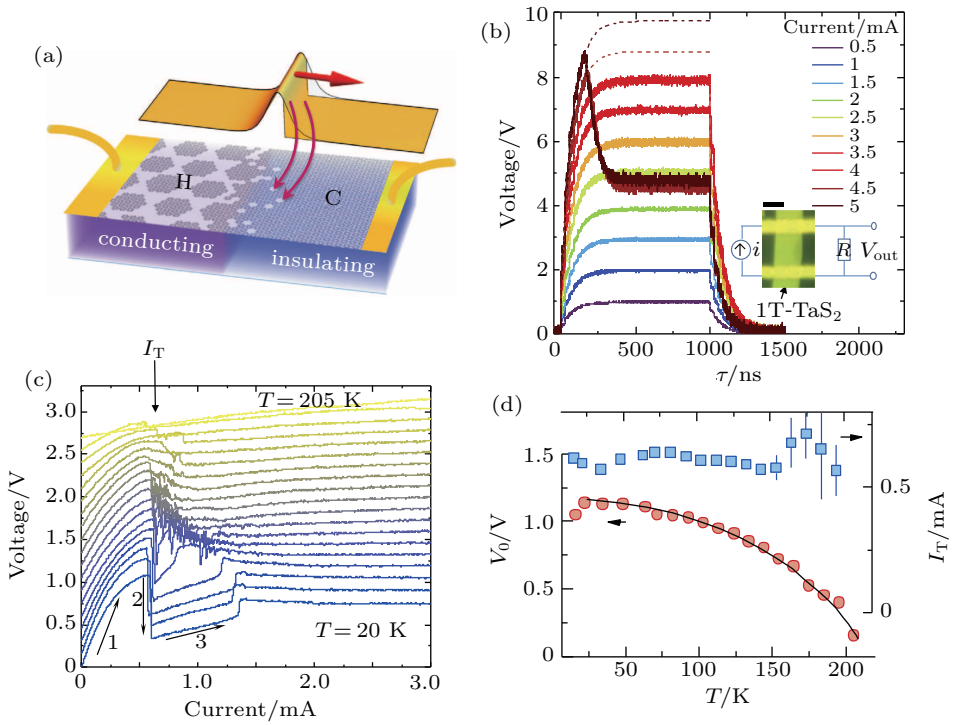


Fig. 6. CDW phase transition driven by electrical pulse. (a) The phase transition can be driven by electrical pulse. As an electrical pulse travels through the sample, the melting of C phase occurs to generate highly conductive hidden states. (b) Temporal response of 1T-TaS_2 by applying a current pulse. (c) The pulsed V–I characteristic at different temperatures. (d) The temperature-dependent V_0 and I_T. V_0 is the voltage at $I = 0$ mA and I_T is the threshold current for the phase transition. This figure was reproduced from Ref. [39] with permission. Copyright 2016, Springer Nature.

During the current pulse triggered phase transition, there are several characteristics. First, with the increase of current density of electrical pulse, an abrupt drop of electrical resistance occurs in 1T-TaS_2, indicating the phase transition from a Mott insulator to a highly conductive metallic state (Fig. 6(b)). Second, the CDW phase switching is strongly dependent on the pulse duration time. For pulses with duration time higher than 0.1 ps, phase switching is incomplete or cannot occur.

The measurable phase switching speed can reach 30 ps. Third, electrical-pulse-driven phase transition presents a significant dependence on temperature (Figs. 6(c) and 6(d)). The obvious switching only occurs with temperature ranging from 10 K to 55 K. In the range of 55 K to 165 K, unstable voltage response was observed above a threshold current. Based on these facts, Vaskivskyi *et al.* proposed a mechanism based on the formation of a hidden state similar to the femtosecond laser pulse excitation.[39] The injected charges can cause the partial collapse of the David-star clusters and the establishment of organized David-star domains separated by conductive domain walls.

Optical pulses and electric field can drive CDW phase transitions in 1T-TaS_2. However, the mechanism for the phase transition triggered by electric field and optical pulses is still under debate. Recently, Shao *et al.* studied the electron and hole doping of 1T-TaS_2 by using density-functional-theory (DFT) calculations.[43] They found that the stability of CDW domains can be suppressed by hole doping which weakens the electron density at the center of star-of-David, while the stability of CDW phase is not sensitive to electron doping.

Compared to the out-of-plane electric field, the phase-transition mechanisms driven by optical pulses and in-plane electric field are more complex and still under debate. Two mechanisms are proposed. First, optical excitation and in-plane electric field can inject mobile holes in 1T-TaS_2, which triggers the melting of star-of-David. Second, light irradiation and electrical current can generate Joule heat, giving rise to the increase of local temperature over the phase-transition point. By measuring the Stokes and anti-Stokes Raman spectra of 1T-TaS_2 during the phase-transition process driven by in-plane electric field,[44] we found that the local temperatures range from 295 K to 320 K, which excludes the Joule heating mechanism in this case.

4. Bolometers based on CDW phase transitions in 1T-TaS_2

The CDW phase switching can be driven by light irradiation in 1T-TaS_2, thus leading to their practical application as photodetectors. In contrast from semiconductors with a finite bandgap and thus the photodetectors with a narrow spectral response, the photodetection based on phase transition possess a broadband response. Due to its metallic nature, 1T-TaS_2 exhibits broadband light absorption with wavelength ranging from several hundreds of nanometers to 100 micrometers (Fig. 7(a)).

Before discussing the photodetection applications, we briefly summarize the synthesis methods for high-quality 1T-TaS_2 two-dimensional (2D) nanoflakes, which is important for scalable construction of high-performance devices. Mechanical exfoliated nanoflakes exhibit high crystallinity, but their practical device applications are limited by the low fabrication efficiency. The chemical vapor deposition (CVD) method has been employed to fabricate 1T-TaS_2. Liu and his colleagues demonstrated that few-layer 1T-TaS_2 can be grown by CVD.[45] Huang *et al.* synthesized vertically oriented 1T-TaS_2 with abundant edge sites on nanoporous gold substrates.[46] Xie *et al.* also demonstrated the CVD growth of 1T-TaS_2 on h-BN substrate.[30] These results provide the possibility for scalable fabrication of high-performance devices based on CDW phase transition.

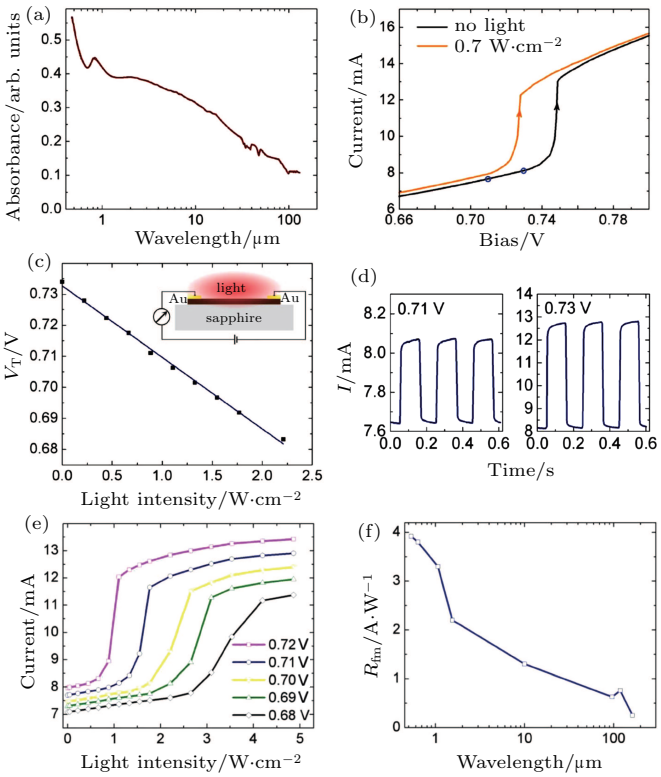


Fig. 7. Photodetectors based on the CDW phase transition in 1T-TaS_2. (a) Absorption spectrum of 1T-TaS_2. (b) The *I*–*V* curves of 1T-TaS_2 at the dark state and the light illumination of 0.7 W·cm^{-2}. (c) Voltage threshold of NC-to-IC phase transition under different light irradiance. (d) The time response of photodetectors under the light pulse of 5 Hz and 0.7 mW·cm^{-2}. (e) The current of device under different light intensities. (f) Spectral response of photodetector. This figure was reproduced from Ref. [47] with permission. Copyright 2018, AAAS.

At room temperature, the phase transition from NC-to-IC states can be triggered by an ultrafast femtosecond laser pulse with a threshold of light intensity. In contrast, Wu *et al.* demonstrated that the sliding of C domain under the applied electric field can be manipulated by applying light with much lower power, reflected by the striking decrease of threshold voltage for the NC-to-IC phase transition (Fig. 7(b)).[47] The decrease of threshold voltage is linearly dependent on the light intensity and the good linearity enables the high-performance light sensing (Fig. 7(c)). The abrupt rise and decay of electrical current were observed in 1T-TaS_2 by applying a 5-Hz pulsed light (Fig. 7(d)), suggesting the fast temporal response of this photodetector. Wu *et al.* also studied the evolution of

device current with the light intensity at different applied voltages and the wavelength-dependent responsivity (Figs. 7(e) and 7(f)). The highest responsivity can achieve ~ 4 A·W^{-1} for this photodetector. Even under light with wavelength of 10 μm, the photoresponsivity exceeds 1 A·W^{-1}. Therefore, due to the lack of bandgap for 1T-TaS_2 at room temperature, it is an ultra-broadband photodetector with relatively high response. Since the sliding of CDW domains requires some lattice distortion, the photodetector exhibits ultrahigh response speed. The rise and decay times were recorded as ~ 1.5 ns and 30 ns, respectively.

The ultrathin nature of suspended 2D 1T-TaS_2 film can have ultralow thermal capacitance and then has extremely high bolometric response. Xie and his colleagues demonstrated highly responsive bolometers based on suspended 1T-TaS_2. The as-grown 1T-TaS_2 film (around 100 nm thick) exhibits broadband optical absorption with relatively low transmittance ranging from 20% to 40% (Fig. 8(a)). Devices were fabricated by suspending of 1T-TaS_2 and a pair of metal electrodes (Fig. 8(b)). Interestingly, the bolometric effect can contribute to the NC-to-IC phase transition process. At voltages ranging from 0.5 V to 1.4 V, prominent decrease of resistance was observed under applied infrared light (Fig. 8(c)). For applied voltage exceeding 1.3 V, the resistance of 1T-TaS_2 experienced a significant reduction. When the applied voltage increased to 1.5 V, the change was hard to be observed, caused by the buildup of IC phase under the applied voltage. Therefore, incident photons can heat up the 1T-TaS_2 and contribute to the NC to IC phase transition through the bolometric effect.

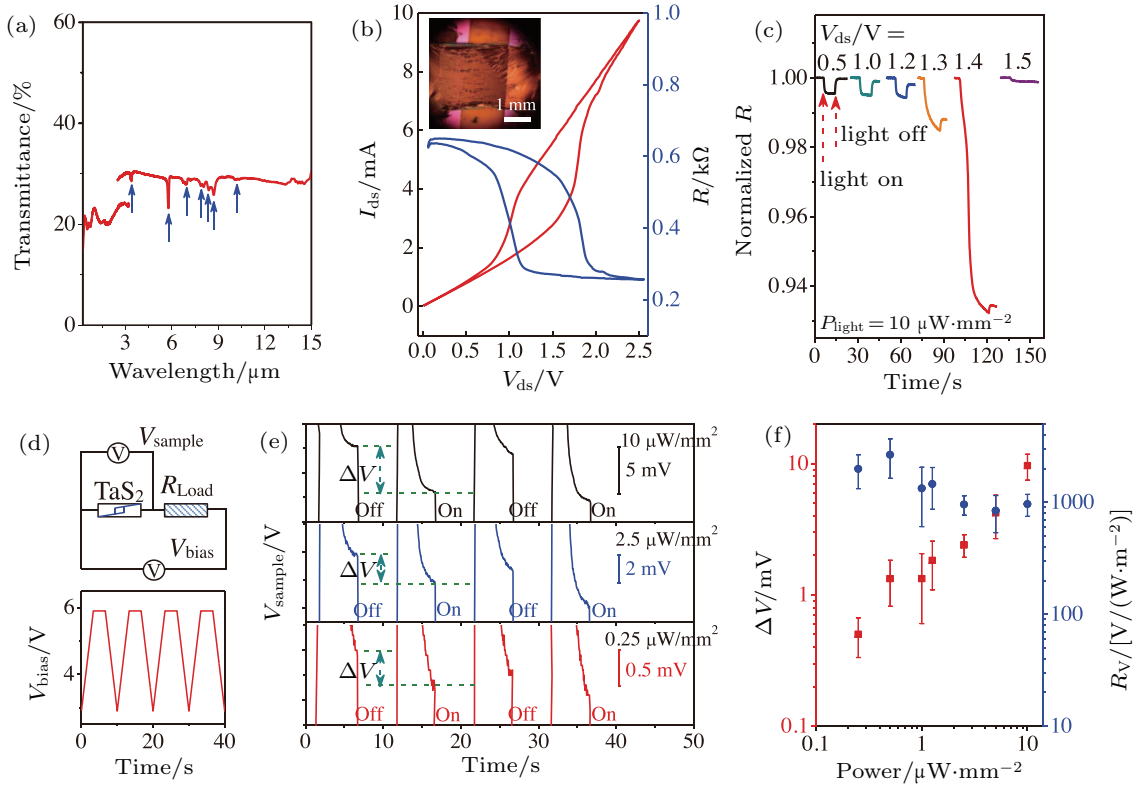


Fig. 8. Bolometric performance of a 1T-TaS_2 film. (a) Transmittance spectrum of 1T-TaS_2. (b) Current and resistance of 1T-TaS_2 at different applied voltages. (c) Bolometric resistance response of 1T-TaS_2 under IR light with irradiance of 10 μW·mm^{-2} at different applied voltages. (d) Scheme of circuit and the AC electrical waveform used in the voltage responsivity measurements. (e) Voltage response at different IR irradiance. (f) Derived voltage and responsivity under different illumination powers. This figure is reproduced from Ref. [30] with permission. Copyright 2018, Wiley-VCH.

The figures of merit of 1T-TaS_2 bolometers were evaluated by constructing a circuit, in which 1T-TaS_2 was connected in serial with a load resistor. An alternating current (AC) bias was supplied to tune the phase transition of 1T-TaS_2 (Fig. 8(d)). Under light irradiation, a striking voltage drop of 1T-TaS_2 was observed due to the decrease of resistance. The responsivity R_V is calculated by $R_V = V_{resp}/P_{light}$, where V_{resp} is the voltage difference before and after light irradiation and P_{light} is the light power. A highest responsivity of 2600 V·W^{-1}·mm^2 was observed, which is higher than that of other bolometers that are based on strongly correlated phase transition, such as VO_X and semiconducting yttrium barium copper oxide (YBCO).

5. Conclusion and perspectives

Extensive research has been made in CDW phase transitions and their dynamics: from ultrafast melting of CDW domains to the buildup of out-of-equilibrium hid-

den/intermediate states. The phase transition processes, including the melting of David-star domains and the buildup of new phase, are accompanied with the striking change of electrical conductivity. Fertile CDW phases and their striking contrast of electrical conductivity offer an interesting avenue to create multifunctional devices, including photodetectors. Photodetection based on strongly correlated electronic system is strikingly different from conventional semiconductors. Without a bandgap, the CDW-based photodetectors can exhibit broadband photodetection with wavelength ranging from several hundreds of nanometers to hundreds of micrometers. The ultrafast melting, nucleation, and growth of CDW ordering offer a core opportunity for the fabrication of ultrafast devices. Although the potential photodetection application of 1T-TaS_2 has been outlined in this review, research on CDW-based photodetectors is still preliminary.

First, the mechanism of the photoresponse is still unclear. The photodetectors operated at room temperatures should originate from the NC to IC phase transition. The lattice dynamics research is carried out by employing femtosecond optical excitation, in which high fluence of photons are injected into 1T-TaS_2 within ultra-short time. However, photodetection experiments are usually performed under continuous wave light excitation with relatively lower fluence, which cannot achieve the ultrafast melting of CDW ordering without the help of the applied electric field. Therefore, the underlying mechanisms for the CDW phase transition driven by femtosecond laser pulse and continuous wave light are possibly different. In this respect, further studies into the lattice dynamics under electric field and continuous wave light excitation should be carried out to reveal the underlying mechanism.

Second, the signal-to-noise ratio of the CDW-based photodetectors need to be further improved. Currently, 1T-TaS_2 is still highly conductive even at the dark condition, which is due to the conductive domain walls in the NCCDW phase as well as the small CDW gaps. So further research is needed to find CDW materials with a much lower conductivity in the ground CDW state and a much higher conductivity in the excited state. We believe that the concept of photodetection based on the CDW phase transition offers new opportunities for creating high-performance photodetectors with broadband spectral sensitivity, ultrafast response, and an ultrahigh signal-to-noise ratio.

References

[1] Yang H, Kim S W, Chhowalla M and Lee Y H 2017 *Nat. Phys.* **13** 931

[2] Keimer B and Moore J E 2017 *Nat. Phys.* **13** 1045

[3] Wang Y, Xiao J, Zhu H, Li Y, Alsaid Y, Fong K Y, Zhou Y, Wang S, Shi W, Wang Y, Zettl A, Reed E J and Zhang X 2017 *Nature* **550** 487

[4] Yi S, Zhang Z and Cho J H 2018 *Phys. Rev. B* **97** 041413

[5] Wilson J A, Disalvo F J and Mahajan S 1975 *Adv. Phys.* **24** 117

[6] Gruner G 1988 *Rev. Mod. Phys.* **60** 1129

[7] Xi X X, Zhao L, Wang Z F, Berger H, Forro L, Shan J and Mak K F 2015 *Nat. Nanotechnol.* **10** 765

[8] Porer M, Leierseder U, Menard J M, Dachraoui H, Mouchliadis L, Perakis I E, Heinzmann U, Demsar J, Rossnagel K and Huber R 2014 *Nat. Mater.* **13** 857

[9] Huang C, Zhang E, Yuan X, Wang W, Liu Y, Zhang C, Ling J, Liu S and Xiu F 2017 *Chin. Phys. B* **26** 067302

[10] Navarro-Moratalla E, Island J O, Manas-Valero S, Pinilla-Cienfuegos E, Castellanos-Gomez A, Quereda J, Rubio-Bollinger G, Chirolli L, Silva-Guillen J A, Agrait N, Steele G A, Guinea F, van der Zant H S J and Coronado E 2016 *Nat. Commun.* **7** 11043

[11] Sipos B, Kusmartseva A F, Akrap A, Berger H, Forro L and Tutis E 2008 *Nat. Mater.* **7** 960

[12] Wei L L, Sun S S, Sun K, Liu Y, Shao D F, Lu W J, Sun Y P, Tian H F and Yang H X 2017 *Chin. Phys. Lett.* **34** 086101

[13] Yu Y, Yang F, Lu X F, Yan Y J, Cho Y H, Ma L, Niu X, Kim S, Son Y W, Feng D, Li S, Cheong S W, Chen X H and Zhang Y 2015 *Nat. Nanotechnol.* **10** 270

[14] Yoshida M, Suzuki R, Zhang Y J, Nakano M and Iwasa Y 2015 *Sci. Adv.* **1** e1500606

[15] Cho D, Gye G, Lee J, Lee S H, Wang L, Cheong S W and Yeom H W 2017 *Nat. Commun.* **8** 392

[16] Cho D, Cheon S, Kim K S, Lee S H, Cho Y H, Cheong S W and Yeom H W 2016 *Nat. Commun.* **7** 10453

[17] Ma L G, Ye C, Yu Y J, Lu X F, Niu X H, Kim S, Feng D L, Tomanek D, Son Y W, Chen X H and Zhang Y B 2016 *Nat. Commun.* **7** 10956

[18] Cho D, Cho Y H, Cheong S W, Kim K S and Yeom H W 2015 *Phys. Rev. B* **92** 085132

[19] Dong L, Wang G Y, Zhu Z, Zhao C X, Yang X Y, Li A M, Chen J L, Guan D D, Li Y Y, Zheng H, Xie M H and Jia J F 2018 *Chin. Phys. Lett.* **35** 066801

[20] Lahoud E, Meetei O N, Chaska K B, Kanigel A and Trivedi N 2014 *Phys. Rev. Lett.* **112** 206402

[21] Shen W, Ge Y Z, Liu A Y, Krishnamurthy H R, Devereaux T P and Freericks J K 2014 *Phys. Rev. Lett.* **112** 176404

[22] Ligges M, Avigo I, Golez D, Strand H U R, Beyazit Y, Hanff K, Diekmann F, Stojchevska L, Kallane M, Zhou P, Rossnagel K, Eckstein M, Werner P and Bovensiepen U 2018 *Phys. Rev. Lett.* **120** 166401

[23] Hellmann S, Beye M, Sohrt C, Rohwer T, Sorgenfrei F, Redlin H, Kallane M, Marczynski-Buhlow M, Hennies F, Bauer M, Fohlisch A, Kipp L, Wurth W and Rossnagel K 2010 *Phys. Rev. Lett.* **105** 187401

[24] Perfetti L, Loukakos P A, Lisowski M, Bovensiepen U, Wolf M, Berger H, Biermann S and Georges A 2008 *New J. Phys.* **10** 053019

[25] Haupt K, Eichberger M, Erasmus N, Rohwer A, Demsar J, Rossnagel K and Schwoerer H 2016 *Phys. Rev. Lett.* **116** 016402

[26] Laulhe C, Huber T, Lantz G, Ferrer A, Mariager S O, Grubel S, Rittmann J, Johnson J A, Esposito V, Lubcke A, Huber L, Kubli M, Savoini M, Jacques V L R, Cario L, Corraze B, Janod E, Ingold G, Beaud P, Johnson S L and Ravy S 2017 *Phys. Rev. Lett.* **118** 247401

[27] Vogelgesang S, Storeck G, Horstmann J G, Diekmann T, Sivis M, Schramm S, Rossnagel K, Schafer S and Ropers C 2018 *Nat. Phys.* **14** 184

[28] Albertini O R, Zhao R, McCann R L, Feng S, Terrones M, Freericks J K, Robinson J A and Liu A Y 2016 *Phys. Rev. B* **93** 214109

[29] Zhao R, Wang Y, Deng D, Luo X, Lu W J, Sun Y P, Liu Z K, Chen L C and Robinson J 2017 *Nano Lett.* **17** 3471

[30] Wang X S, Liu H N, Wu J X, Lin J H, He W, Wang H, Shi X H, Suenaga K and Xie L M 2018 *Adv. Mater.* **30** 1800074

[31] He R, Okamoto J, Ye Z, Ye G, Anderson H, Dai X, Wu X, Hu J, Liu Y, Lu W, Sun Y, Pasupathy A N and Tsen A W 2016 *Phys. Rev. B* **94** 201108

[32] Hu Q, Yin C, Zhang L, Lei L, Wang Z, Chen Z, Tang J and Ang R 2018 *Chin. Phys. B* **27** 017104

[33] Liu G X, Rumyantsev S, Bloodgood M A, Salguero T T and Balandin A A 2018 *Nano Lett.* **18** 3630

[34] Liu G X, Debnath B, Pope T R, Salguero T T, Lake R K and Balandin A A 2016 *Nat. Nanotechnol.* **11** 845

[35] Zhu C, Chen Y, Liu F C, Zheng S J, Li X B, Chaturvedi A, Zhou J D, Fu Q D, He Y M, Zeng Q S, Fan H J, Zhang H, Liu W J, Yu T and Liu Z 2018 *ACS Nano* **12** 11203

[36] Yoshida M, Gokuden T, Suzuki R, Nakano M and Iwasa Y 2017 *Phys. Rev. B* **95** 121405
[37] Stojchevska L, Vaskivskyi I, Mertelj T, Kusar P, Svetin D, Brazovskii S and Mihailovic D 2014 *Science* **344** 177
[38] Vaskivskyi I, Gospodaric J, Brazovskii S, Svetin D, Sutar P, Goreshnik E, Mihailovic I A, Mertelj T and Mihailovic D 2015 *Sci. Adv.* **1** e1500168
[39] Vaskivskyi I, Mihailovic I A, Brazovskii S, Gospodaric J, Mertelj T, Svetin D, Sutar P and Mihailovic D 2016 *Nat. Commun.* **7** 11442
[40] Hollander M J, Liu Y, Lu W J, Li L J, Sun Y P, Robinson J A and Datta S 2015 *Nano Lett.* **15** 1861
[41] Tsen A W, Hovden R, Wang D, Kim Y D, Okamoto J, Spoth K A, Liu Y, Lu W, Sun Y, Hone J C, Kourkoutis L F, Kim P and Pasupathy A N 2015 *Proc. Natl. Acad. Sci. USA* **112** 15054
[42] Cao Y F, Cai K M, Li L J, Lu W J, Sun Y P and Wang K Y 2014 *Chin. Phys. Lett.* **31** 077203
[43] Shao D F, Xiao R C, Lu W J, Lv H Y, Li J Y, Zhu X B and Sun Y P 2016 *Phys. Rev. B* **94** 125126
[44] Wen W, Zhu Y, Dang C, Chen W and Xie L 2019 *Nano Lett.* **19** 1805
[45] Fu W, Chen Y, Lin J, Wang X, Zeng Q, Zhou J, Zheng L, Wang H, He Y, He H, Fu Q, Suenaga K, Yu T and Liu Z 2016 *Chem. Mater.* **28** 7613
[46] Huan Y H, Shi J P, Zou X L, Gong Y, Zhang Z P, Li M H, Zhao L Y, Xu R Z, Jiang S L, Zhou X B, Hong M, Xie C Y, Li H, Lang X Y, Zhang Q, Gu L, Yan X Q and Zhang Y F 2018 *Adv. Mater.* **30** 1705916
[47] Wu D, Ma Y, Niu Y, Liu Q, Dong T, Zhang S, Niu J, Zhou H, Wei J, Wang Y, Zhao Z and Wang N 2018 *Sci. Adv.* **4** eaao3057